Vol. 40 (2009) ACTA PHYSICA POLONICA B No 2

ELLIPTIC FLOWS OF IDENTIFIED PARTICLES IN NUCLEUS–NUCLEUS COLLISIONS AT HIGH ENERGY

Fu-Hu Liu[†], Jun-Sheng Li

Shanxi University, Taiyuan, Shanxi 030006, China

(Received September 1, 2008; revised version received October 16, 2008)

The dependences of elliptic flows on transverse momentum for identified particles produced in nucleus–nucleus collisions at high energy are studied by using a multi source ideal gas model that describes the distribution of transverse momenta as a Rayleigh-like distribution. The experimental results of Au–Au collisions at $\sqrt{s} = 200A$ and $62.4A$ GeV and Cu–Cu collisions at $\sqrt{s} = 200A$ GeV, measured by the STAR and PHENIX collaborations, are well described by this model.

PACS numbers: 24.10.Pa, 24.10.–i, 25.75.Dw

1. Introduction

High energy nucleus–nucleus collisions are at the interface of the fields of particle and nuclear physics [1-3]. In such collisions, the particle azimuthal anisotropy and its dependence on particle identity and on transverse momentum can provide information on the properties of interacting system [4-6]. Generally, the azimuthal anisotropy is described by the second-harmonic coefficient $v_2 = \langle \exp[i2(\phi - \Psi)] \rangle$ of the Fourier expansion of the azimuthal distribution of produced particles, where ϕ, Ψ, and $\langle \ldots \rangle$ denote the azimuthal angle of a produced particle in laboratory reference frame, the azimuthal angle of the reaction plane in the same frame, and the statistical averaging over particles and events, respectively [7,8].

The second moment of the anisotropy flow v_2 is called the elliptic flow which is observed mainly in semi-central nucleus–nucleus collisions. In such collisions, elliptic flows of different identified particles results from hydrodynamic pressure gradients developed in a locally thermalized "almond-shaped" collision (participant) zone [9]. Many local sources of produced particles are formed in the collisions. Because the interactions exist among local sources (produced particles [9]), the initial transverse coordinate-space anisotropy of the participant region is converted into an azimuthal momentum-space anisotropy [9].

[†] fuhuliu@163.com

Many models have been introduced to describe particle productions in high energy collisions. For example, the FRITIOF model [10], the VENUS model [11,12], the RQMD model [13-15], the Gribov–Glauber model [16], the QGSM model [17], the Hydrodynamics model [18,19], the string percolation model [20], a running coupling non-linear evolution [21], the HIJING model [22-24], the ART model [25], the ZPC model [26], a multiphase transport model (the AMPT model) [27], the color glass condensate (CGC) model [28], the perturbative QCD plus saturation plus hydrodynamics (EKRT) model [29], a consistent quantum mechanical multiple scattering approach (EPOS) [30-31], a combination model of constituent quarks and Landau hydrodynamics [32], a two-stage gluon model or a gluon dominance model [33], the KKT model [34], *etc.* In this paper, we will use our multi source ideal gas model [35-37] to describe the elliptic flow of identified particles produced in nucleus–nucleus collisions at high energy. This model contains anisotropic expansions and displacements of the participant region in the transverse momentum-space. The dependences of elliptic flows on transverse momentum for different identified particles produced in Au–Au collisions at $\sqrt{s} = 200A$ and $62.4A$ GeV and Cu–Cu collisions at $\sqrt{s} = 200A$ GeV will be investigated.

2. The model

Let the beam direction be the oz axis and the reaction plane be the xoz plane. The azimuthal momentum-space anisotropy of particles produced in nucleus–nucleus collisions at high energy can be described by the momentum components p_x and p_y. According to our multi source ideal gas model [35-37], p_x and p_y are regarded as to have Gaussian distributions with the distribution widths σ_1 and σ_2, and the mean values $\langle p_x\rangle$ and $\langle p_y\rangle$, respectively. These distribution widths and mean values relate to expansions and displacements of the participant region respectively.

Considering the expressions of random variables with Gaussian distributions in the Monte Carlo calculation, the transverse momentum is given by

$$\begin{aligned} p_{\mathrm{T}} &= \sqrt{p_x^2+p_y^2} \\ &= \sqrt{\Big[\sigma_1\sqrt{-2\ln R_1}\cos(2\pi R_2)+\langle p_x\rangle\Big]^2+\Big[\sigma_2\sqrt{-2\ln R_3}\cos(2\pi R_4)+\langle p_y\rangle\Big]^2}, \quad (1) \end{aligned}$$

where R_1, R_2, R_3, and R_4 denote random numbers in $[0,1]$. In the case of $\sigma_1 = \sigma_2 = \sigma_0$ and $\langle p_x\rangle = \langle p_y\rangle = 0$, one obtains that p_{T} has a Rayleigh distribution, *i.e.* $p_{\mathrm{T}} = \sigma_0\sqrt{-2\ln R_5}$, where R_5 denotes random numbers in $[0,1]$. The p_{T} distribution obtained using Eq. (1) is called a Rayleigh-like distribution in our model. The azimuthal angle and elliptic flow are given by

$$\varphi = \arctan\frac{p_y}{p_x} = \arctan\frac{\sigma_2\sqrt{-2\ln R_3}\cos(2\pi R_4) + \langle p_y\rangle}{\sigma_1\sqrt{-2\ln R_1}\cos(2\pi R_2) + \langle p_x\rangle} \tag{2}$$

and

$$v_2 = \langle\cos(2\varphi)\rangle\,, \tag{3}$$

respectively. Thus, the dependence of v_2 on $p_{\rm T}$ can be obtained by Eqs. (1)–(3).

To understand the meanings of σ_1 and σ_2, we define $\sigma_1 = k\sigma_2 = k\sigma$, where k is a coefficient that describes the relative expansion degree of the participant region along ox and oy axes. $k = 1$ corresponds to the same expansion along ox and oy axes, and $k > 1$ ($k < 1$) corresponds to a larger expansion along ox (oy) axis. The coefficient k describes also the identity of elliptic flow. Generally speaking, $k = 1$, > 1, and < 1 correspond to zero, positive (in-plane), and negative (out-of-plane) flows, respectively. We may regard k (or σ_1) and σ (or σ_2) as free parameters to be determined by comparison with experimental data. Generally speaking, we may choose a satisfactory coordinate system and have $\langle p_x\rangle = \langle p_y\rangle = 0$.

We do not expect that all measured particles contribute to flow effects. Some particles are isotropically emitted in final state and contribute $\langle v_2\rangle = 0$. This means that we divide final-state particles into two parts: signal and background. The signal particles have a fraction f of concerned particles and contribute to $\langle v_2\rangle \neq 0$; and the background particles have a fraction $1 - f$ and contribute to $\langle v_2\rangle = 0$. The parameter f is the third free parameter in our model.

3. Comparison with experimental data

To identify the validity of Rayleigh-like $p_{\rm T}$ distribution Eq. (1), as an example, Fig. 1 shows the $p_{\rm T}$ distribution, $(1/2\pi p_{\rm T})d^2N/dp_{\rm T}dy$, of ϕ particles produced in Au–Au collisions at $\sqrt{s} = 200A$ GeV. The circles are the STAR experimental data for different centralities [38], with each scaled by the amount indicated in the legend. The dotted curves are our calculated results by Eq. (1) with $\sigma_1 = (1.18\pm0.03)$ GeV/c and $\sigma_2 = (0.26\pm0.01)$ GeV/c. We see that the calculated results are approximately in agreement with the experimental data. It is expected that the comparison will be better if we use a two-component Rayleigh-like distribution. The calculated results by the two-component Rayleigh-like distribution are presented in the figure by the solid curves. The first component corresponds to the low, intermediate, and high $p_{\rm T}$ regions having a contribution of $(98.0 \pm 0.8)\%$ with $\sigma_1 = (1.01\pm0.05)$ GeV/c and $\sigma_2 = (0.39\pm0.09)$ GeV/c. The second component corresponds to the higher $p_{\rm T}$ region having a contribution of $(2.0\pm0.8)\%$ with $\sigma_1 = (1.90\pm0.01)$ GeV/c and $\sigma_2 = (1.40\pm0.01)$ GeV/c. We see a main contribution of the first component.

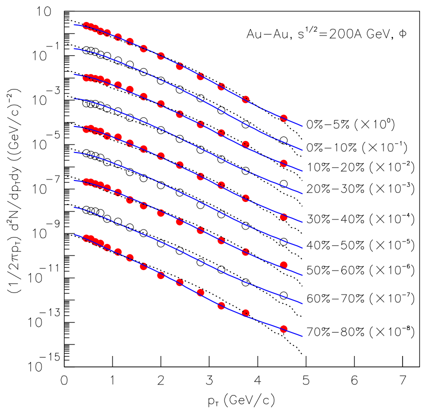

Fig. 1. Transverse momentum distributions of ϕ particles produced in different centralities for Au–Au collisions at $\sqrt{s} = 200A$ GeV. The circles represent the experimental data of the STAR Collaboration [38], with each centrality scaled by the amount indicated in the legend. The curves are our calculated results.

The dependences of elliptic flows on transverse momentum [$v_2(p_T)$] for different identified particles produced in 20%–60% Au–Au collisions at $\sqrt{s} = 200A$ GeV are presented in Fig. 2. The open squares, closed squares, open circles, and closed circles represent the experimental data for $\pi^{\pm}$, $K^{\pm}$, $p(\bar{p})$, and $d(\bar{d})$, respectively [9]. The various curves are our calculated results using Eqs. (1)–(3). In the calculation, the descriptions of the different identified particles result in different parameter values given in Table I with the corresponding χ^2 per degree of freedom (dof). One can see that Eqs. (1)–(3) describe well the measured $v_2(p_T)$ for the four types of particles.

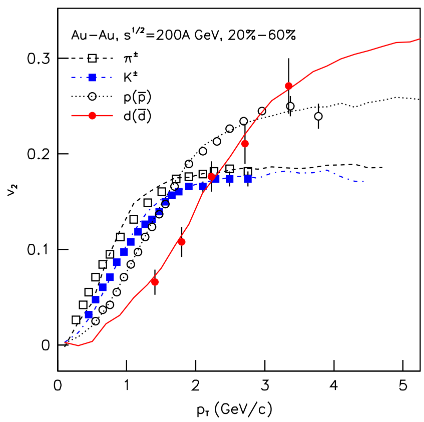

Fig. 2. Dependences of v_2 on p_T for identified particles produced in 20%–60% Au–Au collisions at $\sqrt{s} = 200A$ GeV. The symbols represent the experimental data of the PHENIX Collaboration [9]. The curves are our calculated results by Eqs. (1)–(3).

TABLE I

Parameter values for curves in Figs. 2–10.

Figure	Particle	Centrality	k	σ (GeV/c)	f	χ^2/dof
Fig. 2	$\pi^{\pm}$	20%–60%	4.006	0.333	0.190	0.781
	$K^{\pm}$	20%–60%	2.200	0.375	0.186	0.824
	$p(\bar{p})$	20%–60%	2.198	0.575	0.265	0.337
	$d(\bar{d})$	20%–60%	4.200	1.025	0.350	0.112
Fig. 3	$\pi^{\pm}$	40%–80%	4.320	0.345	0.234	1.298
	$\pi^{\pm}$	10%–40%	4.433	0.320	0.160	0.845
	$\pi^{\pm}$	0%–10%	4.320	0.345	0.080	0.552
Fig. 4	$K^0_{\rm S}$	40%–80%	2.463	0.403	0.191	0.385
	$K^0_{\rm S}$	10%–40%	2.463	0.395	0.150	0.600
	$K^0_{\rm S}$	0%–10%	2.460	0.398	0.069	0.494
Fig. 5	$\Lambda(\bar{\Lambda})$	40%–80%	4.066	0.602	0.285	0.500
	$\Lambda(\bar{\Lambda})$	10%–40%	4.000	0.696	0.225	0.261
	$\Lambda(\bar{\Lambda})$	0%–10%	1.700	0.702	0.125	0.561
Fig. 6	$K^0_{\rm S}$	30%–70%	2.350	0.417	0.203	0.540
	$K^0_{\rm S}$	5%–30%	2.170	0.542	0.160	0.738
	$K^0_{\rm S}$	0%–80%	2.350	0.417	0.147	0.117
	$K^0_{\rm S}$	0%–5%	2.111	0.450	0.056	1.338
Fig. 7	ϕ	40%–80%	2.499	0.733	0.273	0.694
	ϕ	20%–60%	2.348	0.503	0.190	0.201
	ϕ	10%–40%	2.499	0.733	0.243	0.501
	ϕ	0%–80%	2.348	0.503	0.157	0.369
Fig. 8	$\Lambda(\bar{\Lambda})$	30%–70%	2.038	0.625	0.635	0.486
	$\Lambda(\bar{\Lambda})$	5%–30%	2.072	0.709	0.680	0.803
	$\Lambda(\bar{\Lambda})$	0%–80%	2.348	0.715	0.224	0.319
	$\Lambda(\bar{\Lambda})$	0%–5%	2.072	0.709	0.745	1.746
Fig. 9	$h^{\pm}$	40%-5-0%	4.966	0.400	0.236	1.985
	$h^{\pm}$	30%–40%	4.122	0.389	0.215	1.949
	$h^{\pm}$	20%–30%	4.122	0.389	0.185	1.910
	$h^{\pm}$	10%–20%	4.100	0.390	0.145	1.886
	$h^{\pm}$	0%–10%	4.100	0.390	0.088	1.810
Fig. 10	$h^{\pm}$	30%–40%	4.513	0.398	0.160	1.941
	$h^{\pm}$	20%–30%	4.115	0.400	0.150	1.739
	$h^{\pm}$	10%–20%	4.115	0.400	0.134	1.982
	$h^{\pm}$	0%–10%	4.115	0.410	0.115	1.537

Figs. 3, 4, and 5 show respectively a comparison of our model calculation with the experimental results [39] for $\pi^{\pm}$, $K^0_{\rm S}$, and $\Lambda(\bar{\Lambda})$ produced in Au–Au collisions at $\sqrt{s} = 62.4A$ GeV. The parameter values used in the calculation for different centralities are also given in Table I. Once more our simple model describes the experimental data very well.

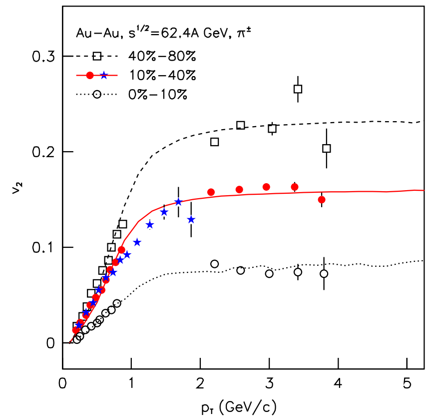

Fig. 3. Dependences of v_2 on p_{T} for $\pi^{\pm}$ produced in Au–Au collisions at $\sqrt{s} = 62.4A$ GeV. The symbols represent the experimental data of the STAR Collaboration [39]. The curves are our calculated results by Eqs. (1)–(3).

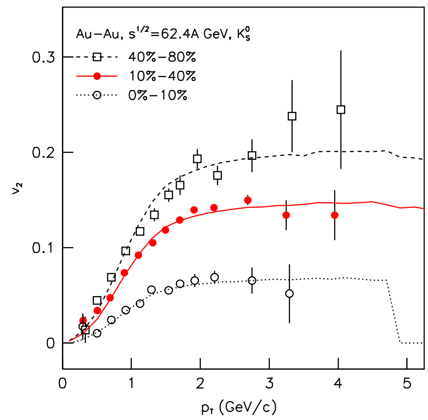

Fig. 4. As for Fig. 3, but showing the results for K^0_{S}.

The dependence of $v_2(p_{\mathrm{T}})$ on centrality for K^0_{S}, ϕ, and $\Lambda(\bar{\Lambda})$ produced in Au–Au collisions at $\sqrt{s} = 200A$ GeV are given in Figs. 6, 7, and 8, respectively, where they are compared to our calculation. The fitted parameter values used in the calculation are given in Table I. One can see that in all cases our model can provide a good description of the experimental data [9,38,40].

In Figs. 9 and 10, the dependence of $v_2(p_{\mathrm{T}})$ on centrality for charged hadrons ($h^{\pm}$) produced in Au–Au and Cu–Cu collisions at $\sqrt{s} = 200A$ GeV are displayed respectively. The fitted parameter values are also given in Table I. One can see that our model describes the experimental data [41].

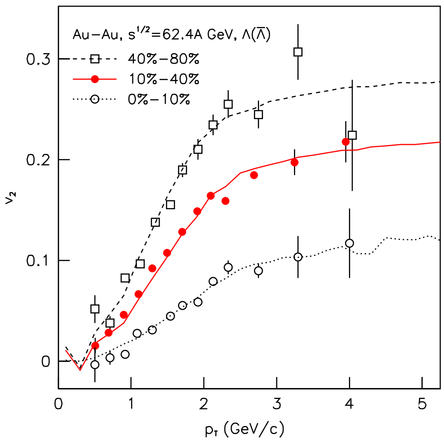

Fig. 5. As for Fig. 3, but showing the results for $\Lambda(\bar{\Lambda})$.

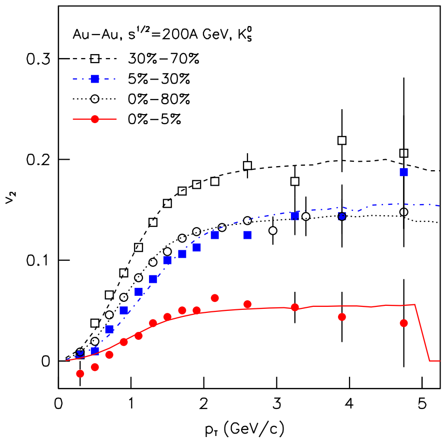

Fig. 6. Dependences of v_2 on $p_{\rm T}$ for $K^0_{\rm S}$ produced in Au–Au collisions at $\sqrt{s} = 200A$ GeV. The symbols represent the experimental data of the STAR Collaboration [38,40]. The curves are our calculated results by Eqs. (1)–(3).

The dependences of the parameter values on particle mass (m) used for centrality 20%–60% in Fig. 2 and 0%–80% in Figs. 6–8 are given in Fig. 11 by different symbols as marked in the figure. The error bars correspond to the estimated relative errors on parameter values of 8%. The curve and lines are fitted results assuming parabolic and linear dependence. One can see that k and σ show obvious dependences on particle mass, while f shows a very slight increase with increasing particle mass. The curves in the figure are given by the relations

$$k = 4.50e^{-2.70m} + 1.10m^{1.80} + 0.82\,, \tag{4}$$

$$\sigma \;=\; 0.40m + 0.20\,, \tag{5}$$

and

$$f = 0.08m + 0.15\,, \tag{6}$$

respectively, with χ^2/dof to be 0.025, 0.293, and 0.950, respectively, where m is in GeV/c^2 and σ in GeV/c.

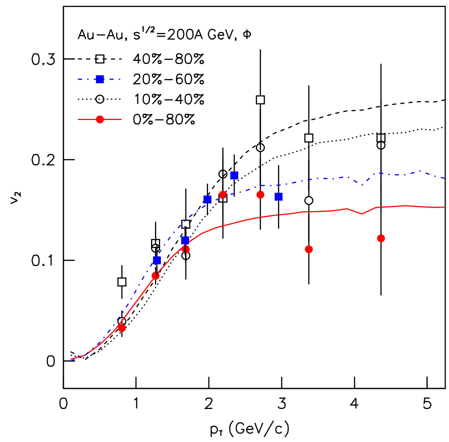

Fig. 7. As for Fig. 6, but showing the results for ϕ. The symbols represent the experimental data of PHENIX and STAR Collaborations [9,38,40].

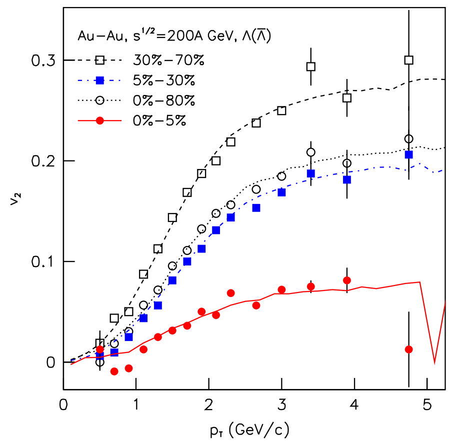

Fig. 8. As for Fig. 6, but showing the results for $\Lambda(\bar{\Lambda})$.

In Fig. 11, we select the centralities 20%–60% and 0%–80% to show the dependences of the parameter values on particle mass because that the centers of the both centralities are the same. For a given type of particle,

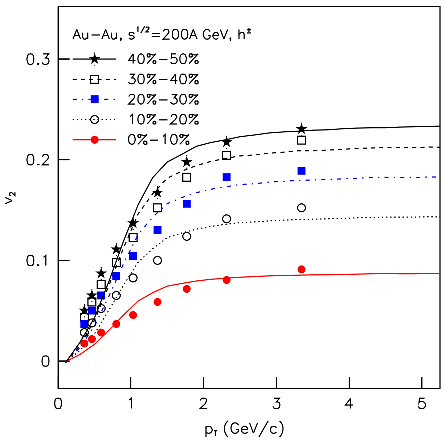

Fig. 9. Dependences of v_2 on p_T for $h^\pm$ produced in Au–Au collisions at $\sqrt{s} = 200A$ GeV. The symbols represent the experimental data of the PHENIX Collaboration [40]. The curves are our calculated results by Eqs. (1)–(3).

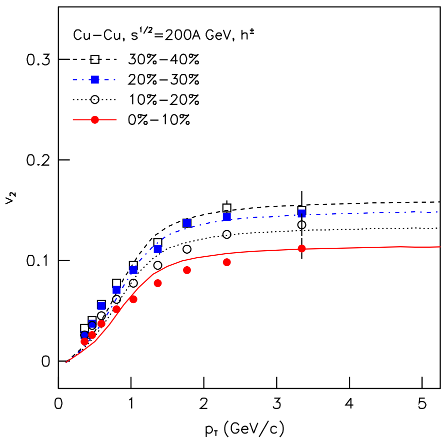

Fig. 10. As for Fig. 9, but showing the results for Cu–Cu collisions.

the identity parameter for the two centralities should have nearly the same value. Except for the mentioned two centralities, others do not have enough particle types to give a comparison.

The parameter values used for Figs. 6–8 are given in Fig. 12, by different symbols as marked in the figure, to see their dependences on centrality. The error bars are the relative errors on parameter values estimated to 8%. One can see that the parameters k and σ do not show an obvious dependence on centrality; and the parameter f shows a slight increase with decreasing centrality. The line in the figure is given by the relation

$$f = 0.30C + 0.09 \tag{7}$$

with χ^2/dof to be 1.439, where C denotes the centrality and is in %.

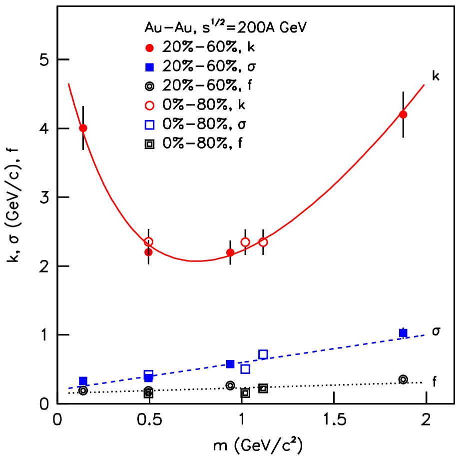

Fig. 11. Dependences of parameter values on particle mass. The symbols represent the parameter values used for centrality 20%–60% in Fig. 2 and 0%–80% in Figs. 6–8. The curve and lines are fitted results.

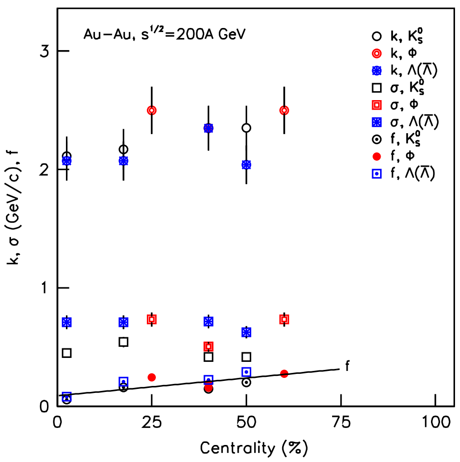

Fig. 12. Dependences of parameter values on centrality. The symbols represent the parameter values used in Figs. 6–8. The line is a fitted result.

To see sensitivities of $v_2(p_{\rm T})$ on parameters, as an example, we show the results of $0.8k$ and $1.2k$, 0.8σ and 1.2σ, as well as $0.8f$ and $1.2f$ in Fig. 13 by the dotted and dashed curves respectively, where the default $k = 3.2$, $\sigma = 0.6$ GeV/c, and $f = 0.1$ gives the solid curve. To display clearly, the results for different k and different σ are given by $+0.2$ and $+0.1$ respectively. One can see that $v_2(p_{\rm T})$ is insensitive to k and sensitive to σ and f. Especially, σ affects mainly the shape of $v_2(p_{\rm T})$; and f affects both the shape and highness.

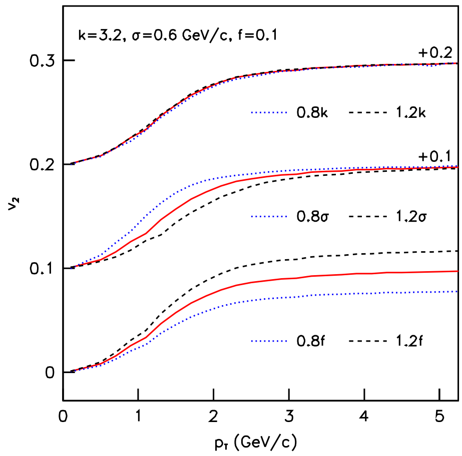

Fig. 13. Sensitivities of $v_2(p_{\rm T})$ on parameters.

4. Conclusion and discussion

To conclude, a multi source ideal gas model is used to give a description of the dependences of elliptic flows on transverse momentum for different identified particles produced in nucleus–nucleus collisions at high energy. The calculated results are compared and found to be in good agreement with the experimental data of Au–Au and Cu–Cu collisions at relativistic heavy ion collider energy.

Three parameters are used in our model. They are a relative strength coefficient k of source expansion, a distribution width σ of momentum component p_y, and a fraction f of signal particles in concerned particles. The present work shows that the parameter k decreases and then increases with increasing particle mass. The parameter σ increases linearly with increasing particle mass. Both the parameters k and σ do not show an obvious dependence on centrality. The parameter f increases slightly with increasing particle mass and decreasing centrality. The $v_2(p_{\rm T})$ is insensitive to k and sensitive to σ and f.

The coefficient k describes a relative expansion degree of the interacting participant region in the transverse plane. $k = 1$, > 1, and < 1 correspond to the same expansion along ox and oy axes, a larger expansion along ox axis, and a larger expansion along oy axis, respectively. The coefficient k is also a description of the identity of elliptic flow. $k = 1$, > 1, and < 1 correspond to non-flow, in-plane positive flow, and out-of-plane negative flow, respectively. The parameter σ describes both the distribution width of p_y and the excitation degree of the concerned source. A physics condition gives $\sigma > 0$. The parameter f is a description of the fraction of signal particles. $f = 0$ corresponds to non-flow owing to zero signal particle. A larger f corresponds to a stronger flow.

From Table I and Fig. 11 we see that the interacting participant concerned in the present work has a larger expansion along ox axis and appears an in-plane positive flow. The strengths of expansion and flow for light and heavy particles are larger than those for intermediate particles. This renders that the light and heavy particles are priori products in the interacting participant. In addition, the mechanics equilibrium of the interacting participant are not mainly contributed by the light (heavy) particles owing to their light masses (small amount).

From Table I and Fig. 11 we see also that the parameters σ and f appear positive values. It is a natural result that the parameter σ increases linearly with increasing particle mass. This causes the light particles to have a narrow p_{T} distribution and the heavy particles to have a wide p_{T} distribution. In the concerned particles, the light particles have a small probability to be signal particles, and the heavy particles have a large fraction to contribute to the flow effect. This renders that the parameter f increases slightly with increasing particle mass.

The authors thank Prof. Jean Barrette for his improvements to the manuscript. The first author thanks the members of the Physics Department of McGill University, Canada, for their hospitality. This work was supported by the China Scholarship Council; the National Natural Science Foundation of China, Grant Nos. 10675077 and 10275042; the Shanxi Provincial Natural (Youth) Science Foundation, Grant Nos. 2007011005 and 20051002; and the Shanxi Provincial Foundation for Returned Overseas Scholars.

REFERENCES

[1] K. Adcox *et al.* [PHENIX Collaboration], *Nucl. Phys.* **A757**, 184 (2005).
[2] M. Gyulassy, L. McLerran, *Nucl. Phys.* **A750**, 30 (2005).
[3] E.V. Shuryak, *Nucl. Phys.* **A750**, 64 (2005).

[4] R.A. Lacey, *Nucl. Phys.* **A774**, 199 (2006).

[5] S.S. Adler *et al.* [PHENIX Collaboration], *Phys. Rev. Lett.* **94**, 232302 (2005).

[6] K.H. Ackermann *et al.* [STAR Collaboration], *Phys. Rev. Lett.* **86**, 402 (2001).

[7] M. Demoulins, D. L'Hôte, J.P. Alard, J. Augerat, R. Babinet, N. Bastid, F. Brochard, C. Cavata, N. De Marco, P. Dupieux, H. Fanet, Z. Fodor, L. Fraysse, P. Gorodetzky, J. Gosset, T. Hayashino, M.C. Lemaire, A. Le Merby, B. Lucas, J. Marroncle, G. Montarou, M.J. Parizet, J. Poitou, C. Racca, W. Schimmerling, Y. Terrien, O. Valette, *Phys. Lett.* **B241**, 476 (1990).

[8] S. Voloshin, Y. Zhang, *Z. Phys.* **C70**, 665 (1996).

[9] S. Afanasiev *et al.* [PHENIX Collaboration], *Phys. Rev. Lett.* **99**, 052301 (2007).

[10] G. Gustafson, *Nucl. Phys.* **A566**, 233c (1994).

[11] K. Werner, *Phys. Rep.* **232**, 87 (1993).

[12] K. Werner, *Nucl. Phys.* **A566**, 477c (1994).

[13] H. Sorge, H. Stöcker, W. Greiner, *Nucl. Phys.* **A498**, 567c (1989).

[14] H. Sorge, A. von Keitz, R. Mattiello, H. Stocker, W. Greiner, *Nucl. Phys.* **A525**, 95c (1991).

[15] A. Jahns, C. Spieles, R. Mattiello, N.S. Amelin, H. Stoecker, W. Greiner, H. Sorge, *Nucl. Phys.* **A566**, 483c (1994).

[16] K. Tywoniuk, I.C. Arsene, L. Bravina, A.B. Kaidalov, E. Zabrodin, `arXiv:0705.1596 [hep-ph]`.

[17] L.V. Bravina, L.P. Csernai, P. Levai, N.S. Amelin, D. Strottman, *Nucl. Phys.* **A566**, 461c (1994).

[18] R.B. Clare, D. Strottmann, *Phys. Rep.* **141**, 177 (1986).

[19] U. Ornik, R.M. Weiner, G. Wilk, *Nucl. Phys.* **A566**, 469c (1994).

[20] J. Dias de Deus, J.G. Milhano, *Nucl. Phys.* **A795**, 98 (2007).

[21] J.L. Albacete, `arXiv:0707.2545 [hep-ph]`.

[22] X.N. Wang, *Phys. Rev.* **D43**, 104 (1991).

[23] X.N. Wang, M. Gyulassy, *Phys. Rev.* **D44**, 3501 (1991).

[24] X.N. Wang, M. Gyulassy, *Phys. Rev. Lett.* **68**, 1480 (1992).

[25] B.A. Li, C.M. Ko, *Phys. Rev.* **C52**, 2037 (1995).

[26] B. Zhang, *Comput. Phys. Commun.* **109**, 193 (1998).

[27] Z.W. Lin, C.M. Ko, B.A. Li, B. Zhang, S. Pal, *Phys. Rev.* **C72**, 064901 (2005).

[28] D. Kharzeev, E. Levin, L. McLerran, *Phys. Lett.* **B561**, 93 (2003).

[29] K.J. Eskola, K. Kajantie, P.V. Ruuskanen, K. Tuominen, *Nucl. Phys.* **B570**, 379 (2000).

[30] H.J. Drescher, M. Hladik, S. Ostapchenko, T. Pierog, K. Werner, *Phys. Rep.* **350**, 93 (2001).

[31] K. Werner, F.M. Liu, T. Pierog, *Phys. Rev.* **C74**, 044902 (2006); K. Werner, *Phys. Rev. Lett.* **95**, 152301 (2007).

[32] E.K.G. Sarkisyan, A.S. Sakharov, `arXiv:hep-ph/0410324`, CERN-PH-TH/2004-213; E.K.G. Sarkisyan, A.S. Sakharov, `arXiv:hep-ph/0510191`; *AIP Conf. Proceedings* **828**, 35 (2006).

[33] E.S. Kokoulina, *Acta Phys. Pol. B* **35**, 295 (2004);
E.S. Kokoulina, V.A. Nikitin, `arXiv:hep-ph/0502224`, talk given at the XVII International Baldin Seminar "Relativistic Nuclear Physics and Quantum Chromodynamics", JINR, Dubna, Russia, Sept. 27–Oct. 2, 2004;
P.F. Ermolov, E.S. Kokoulina, E.A. Kuraev, A.V. Kutov, V.A. Nikitin, A.A. Pankov, I.A. Roufanov, N.K. Zhidkov, `arXiv:hep-ph/0503254` talk given at the XVII International Baldin Seminar "Relativistic Nuclear Physics and Quantum Chromodynamics", JINR, Dubna, Russia, Sept. 27–Oct. 2, 2004.

[34] D. Kharzeev, Y.V. Kovchegov, K. Tuchin, *Phys. Rev.* **D68**, 094013 (2003);
D. Kharzeev, Y.V. Kovchegov, K. Tuchin, *Phys. Lett.* **B599**, 23 (2004).

[35] F.H. Liu, *Europhys. Lett.* **63**, 193 (2003).

[36] F.H. Liu, N.N. Abd Allah, D.H. Zhang, M.Y. Duan, *Int. J. Mod. Phys.* **E12**, 713 (2003).

[37] F.H. Liu, N.N. Abd Allah, B.K. Singh, *Phys. Rev.* **C69**, 057601 (2004).

[38] B.I. Abelev *et al.* [STAR Collaboration], *Phys. Rev. Lett.* **99**, 112301 (2007).

[39] B.I. Abelev *et al.* [STAR Collaboration], *Phys. Rev.* **C75**, 054906 (2007).

[40] J. Adams *et al.* [STAR Collaboration], *Phys. Rev. Lett.* **92**, 052302 (2004).

[41] A. Adare *et al.* [PHENIX Collaboration], *Phys. Rev. Lett.* **98**, 162301 (2007).